Zeus: Mission to Jupiter

Johnathan Clouse*
University of Colorado, Boulder, CO, 80309-0429, USA

*Graduate Student, Aerospace Engineering Sciences, 1111 Engineering Drive, Boulder, CO, 80309-0429

Contents

I. Introduction

Jupiter is the largest planet in the solar system, and the closest gas giant to the sun.

A VEEJ (Venus-Earth-Earth-Jupiter) trajectory was considered for launch in 2020. The requirements are outlined as follows:

The sailcraft's actuator was a gimbaled control boom between the sail subsystem and the spacecraft bus, which contained the majority of the spacecraft mass. With the center of mass between the thrust point and the sun, expected disturbances would cause oscillation about some angle between the sun and the axis normal to the sail, α, for a locked gimbal. Changing the gimbal angle, δ, would dampen this oscillation with the right control law. Roll and pitch angles were held to zero for this analysis. Sun sensors determined spacecraft yaw, and had a maximum error of $\pm 0.05^\circ$.

The state-space model had four states: the sun angle (α), the rate of the sun angle ($\dot{\alpha}$), the gimbal angle (δ), and the gimbal angle rate ($\dot{\delta}$). These states were chosen due to their coupling and resulting output (sun angle), as well as being the only dynamic parameters, as seen in Equations **??** and **??**.The sail and boom were modeled as rigid bodies, justified by the slow actuation of the gimbal throughout the flight. The sail was modeled as a thin plate, rather than a billowed sail. The state-space model was obtained in a similar manner to that presented by Wie.[1] The equations of motion for a gimbaled thrust vector were obtained for the yaw axis.

System performance was judged by the response to errors, namely a step from α=0° to α=35°. Mitigation of disturbance torques was also examined.

II. Preliminary Trajectory Design

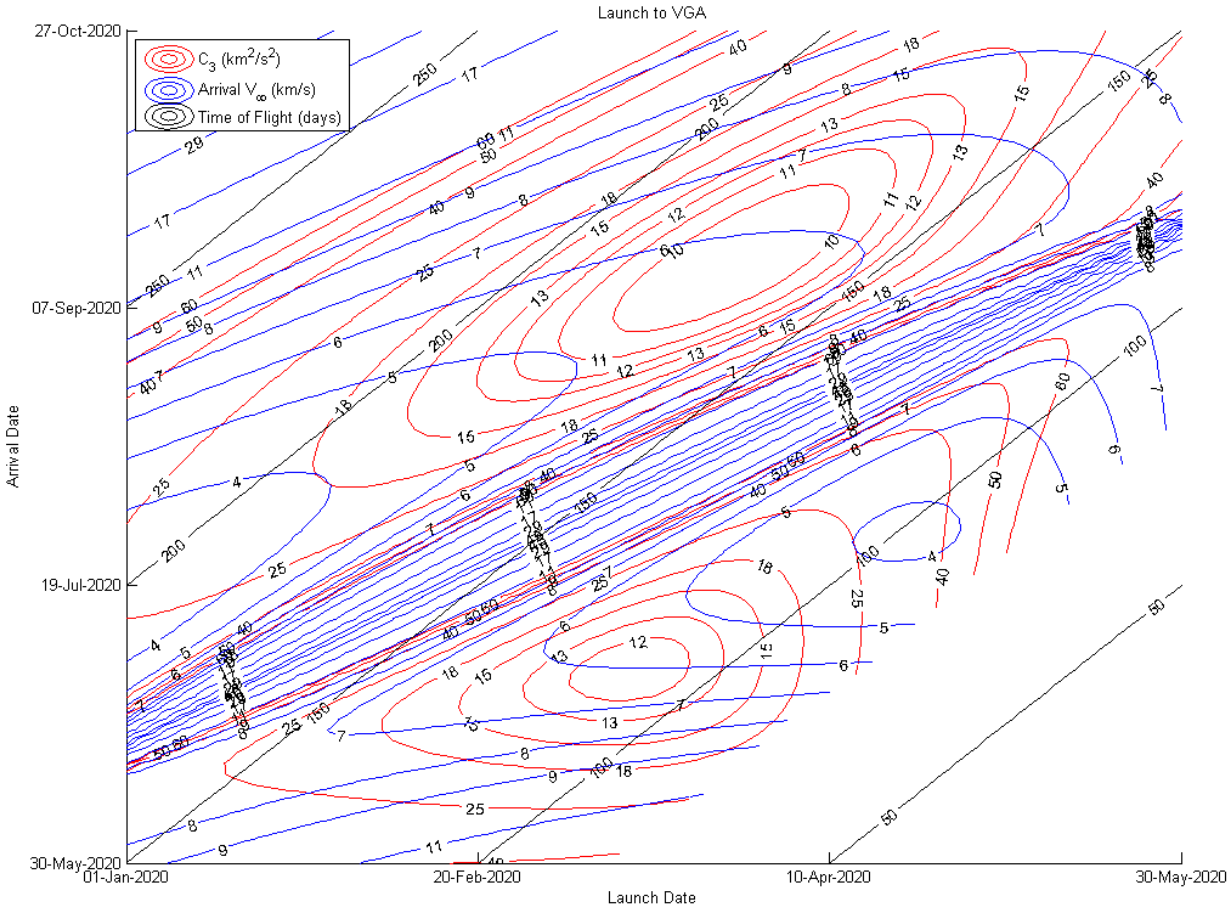

Figure 1. Launch to VGA.

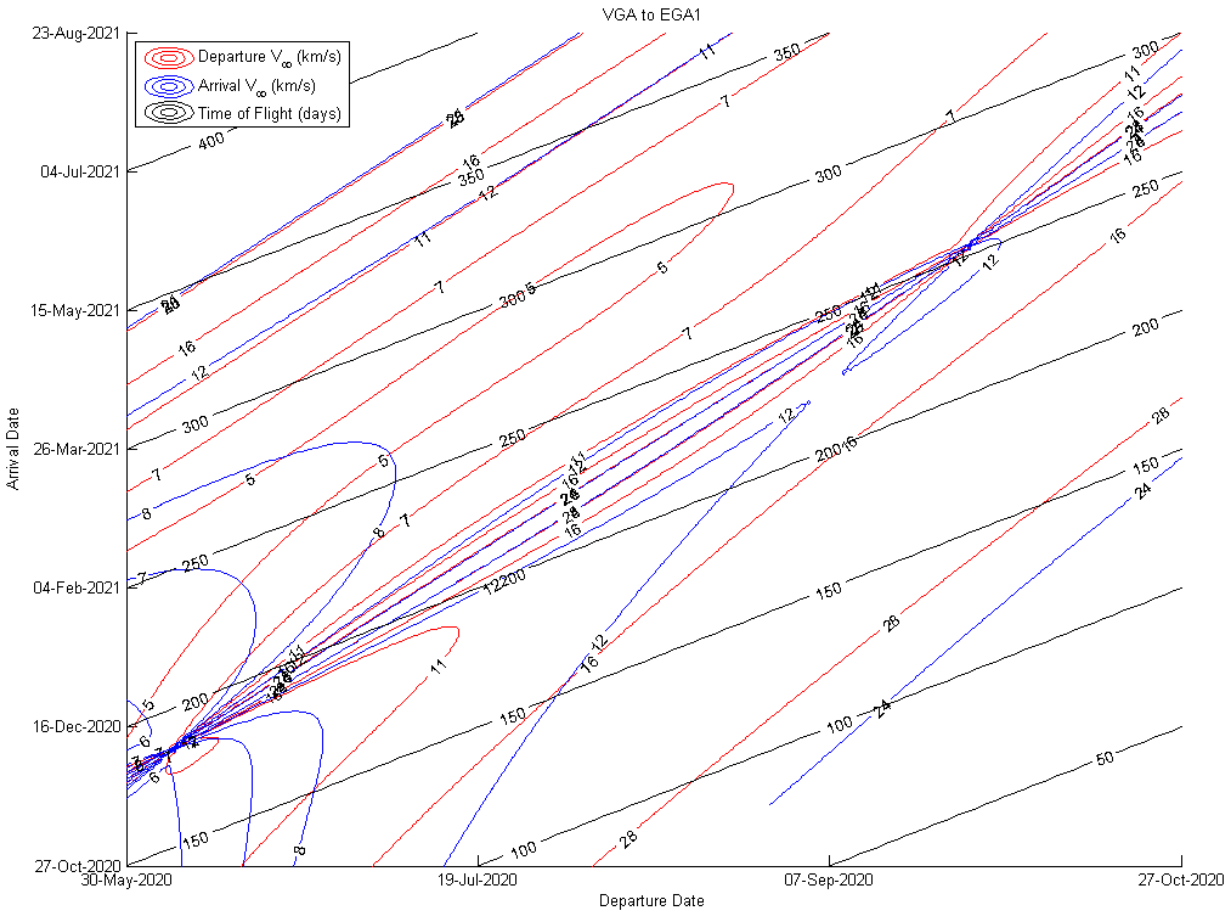

Figure 2. VGA to EGA1.

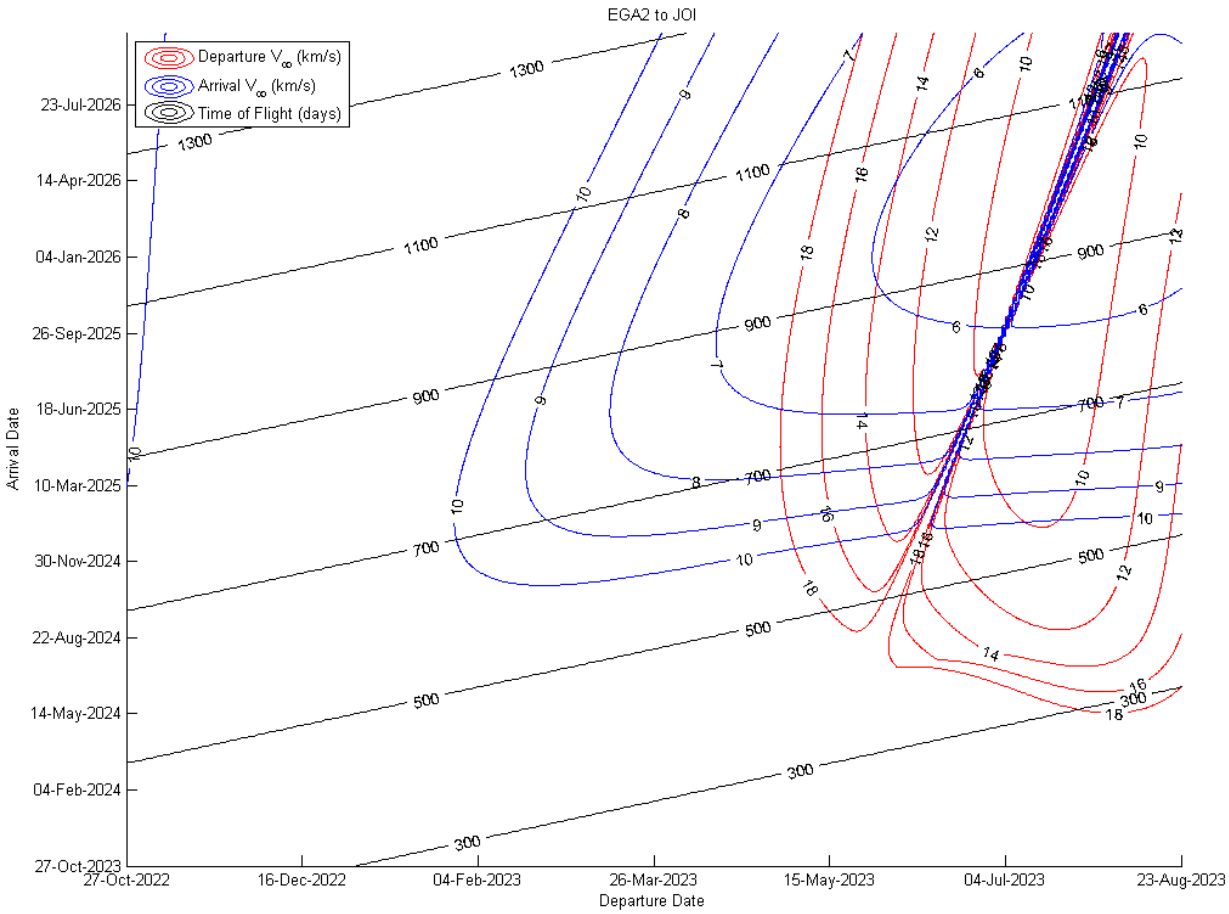

Figure 3. EGA2 to JOI.

Porkchop plots serve as great visual guides to determine low-cost trajectories. However, chaining together multiple gravity assists leads to many potential solutions whose benefits become difficult to compare using several porkchop plots. An algorithm was developed to trim the search space of the possible trajectories, as well as to determine the merits of each trajectory. The algorithm took a predetermined set of windows and determined the lambert solution between the launch, gravity assists, and orbit insertion. Next, launch C3 and final V_∞ were applied to the initial and final windows to rid the search space of known unusable trajectories. The ΔV difference between planetary encounters on a given date were subsequently calculated; any ΔV difference outside of a tuned tolerance were thrown out. The result was a set of dates

Dates were chosen to minimize the V_∞ errors in the calculated gravity assist. Table 1 shows the chosen dates and the relevant targeting parameters.

Table 1. Trajectory parameters

Event	Calendar Date	Julian Date	Information
Launch	25 February 2020 12:52:48	2458906	C_3: 16.72 km^2/s^2 RLA: 108.64° DLA: 7.52° Launched from Tanegashima, Japan
Venus Gravity Assist (VGA)	15 September 2020 12:00:00	2459108	r_p: 23224 km B_T: 29790 B_R: 4735.7 Turning Angle: 29.63° V_∞: 6.39 km/s ΔV_∞: 2.7298e-4 km/s
Resonant Orbit	–	–	Resonance: 2:1 φ: 130.06° V_∞: 9.45 km/s ΔV_∞: 2.7298e-4 km/s
Earth Gravity Assist 1 (EGA1)	12 July 2021 12:00:00	2459408	r_p: 6745.2 km B_T: -7069.2 km B_R: -7474.7 km Turning Angle: 47.00°
Earth Gravity Assist 2 (EGA2)	12 July 2023 12:00:00	2460138	r_p: 7079.5 km B_T:-10549 km B_R: 1472.1 km Turning Angle: 45.56°
Jupiter Orbit Insertion (JOI)	14 February 2026 12:00:00	2461086	V_∞: 5.5868 km/s ΔV: 1.5336 km/s $\left\vert\vec{B}\right\vert$: 3.1108e6 km Inclination: 0° r_p: 1.0711e6 km r_a: 1.4707e7 km Period: 143.1 days

As Table 1 shows, the ΔV_∞ is quite low for each gravity assist. The resonant orbit gravity assist's ΔV_∞ is the error between the initial approach and final departure; the V_∞ magnitude between these times is assumed to be within this error. Because the errors were non-zero, trajectory correction maneuvers (TCM) will have to be performed to allow the spacecraft to reach the calculated B-plane targets. The flyby altitude for each planet is greater than 300 km. Not only does this prevent planetary impact, it reduces drag that a TCM would have to correct. With Earth encounters, conjunction analysis should be performed to ensure there is no risk to hitting another spacecraft. In addition, one must ensure that the Moon does not interfere with or stand in the way of the trajectory. TCMs will have to account for lunar perturbations.

The resonant orbit periapses are shown in Figure 4 below.

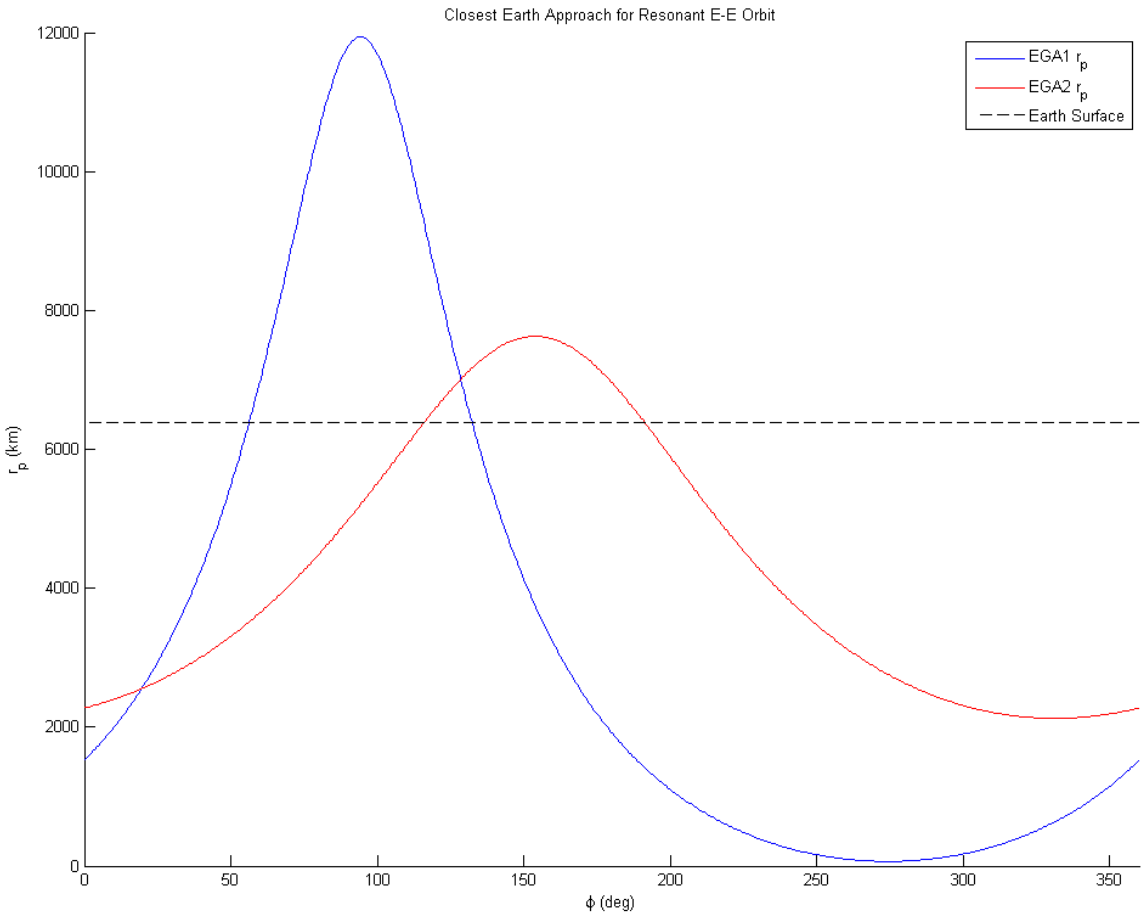

Figure 4. Resonant orbit periapses.

The range of φ that prevents planetary impact for both gravity assists is small. The value of φ was chosen approximately where the periapses are the same (and greater than the radius of Earth) to ensure minimum drag effects on both flybys.

Jupiter's moons can provide both scientific targets and gravity assists. Ganymede, being the most massive body, has been identified as the most useful Jovian moon for changing the spacecraft period.[2] This moon is outside the worst of Jupiter's radiation, making its orbit safe for spacecraft perijove. Ganymede's orbital radius is 1.0711e6 km in radius from Jupiter with an eccentricity of 0.001.[2] Choosing a 20:1 resonant initial orbit with Ganymede gave the spacecraft an apojove of 1.4707e7 km and period of 143.1 days, requiring a JOI ΔV of 1.5336 km/s. Larger initial orbits substantially increased the period while encountering diminishing returns with the JOI ΔV. This initial orbit could allow for a varietry of moon tours that would lower apojove and allow easier capture around one of the moons. In addition, the outer Galilean moons could reduce the JOI burn required. For this trajectory, Ganamede could provide a turning angle of up to 11°. To find the magnitude of $\vec{B}$, one merely computes the hyperbola equation $b = a\sqrt{e^2 - 1}$ to find that $\left|\vec{B}\right| = 3.1108\text{e}6$ km.

A Hohmann transfer from Earth to Jupiter was constructed using semimajor axes of the planets given by Vallado[3] and assuming circular planetary orbits. It is shown alongside the trajectory requirements and the actual performance in Table 2 below.

Table 2. Trajectory requirements

Parameter	Requirement	Actual	Hohmann
Time of flight (years)	<10	6	2.7
C3 (km^2/s^2)	<18	16.72	77.31
Arrival V_∞ (km/s)	<6	5.59	5.64
Total ΔV_∞ (km/s)	<0.3	2.65e-4	N/A

The Hohmann transfer to Jupiter looked attractive due to the shorter time of flight, but the C_3 is prohibitively large. In fact, it's off the chart given by Vallado.[3] The proposed trajectory is most easily compared to the Galileo mission. Galileo was flown to study Jupiter and its moons; one could surmise that the mass of the spacecraft would be comparable. Like the proposed trajectory, Galileo took advantage of a VEEGA. Galileo's time of flight was just over six years. It also had a maximum C_3 of 17 km^2/s^2.[2] With a V_∞ error orders of magnitude less than the maximum allowable, this trajectory was determined to be feasible. The primary difference between this trajectory and Galileo's was its JOI ΔV of 0.630 km/s. Galileo flew by Europa and Io to reduce its jovecentric velocity. As previously discussed, moon flybys could reducd the JOI ΔV required by this trajectory.

III. STK Simulation

The previously documented trajectory was visualized in STK 10. STK allows for simulations of spacecraft and ground facilities to give mission planners much of what they need to detail the spacecraft operations. It computes access between spacecraft and facilities. With the Astrogator package, STK assists in targeting interplanetary trajectories. It can take a savvy mission designer to know the best ways to target a trajectory, but the visualization and reports make communication to spacecraft designers easy. However, STK lacks the ability to search for trajectories given the requirements for this project. Therefore, one must create a trajectory in a similar fashion as described above. STK does allow for custom plugins, which could allow the STK application to be more capable.

Planetery ephemerides were from DE421. Launch was originally targeted at Cape Canaveral, but there was diffuculty in targeting the desired launch declination. Baikonur was the second choice, but the launch intersected Earth on its way out. Tanegashima successfully launched the spacecraft. Tanegashima is 2° above Cape Canaveral, so they are relatively similar for launch purposes. Tanegashima can host interplanetary-bound spacecraft, but assuming Zeus is an American mission, there are regulatory constraints to launch from there.

TCMs were targeted 10 days after each planetary flyby. This time period was found to be far enough from the previous planetary encounter that third-body effects would be small in the overall propagation. Being quite early in the segment, TCM ΔV was kept low. The TCMs are outlined in Table 3 below.

Table 3. STK Trajectory Correction Maneuvers

Maneuver	Calendar Date	Julian Date	ΔV (km/s)
TCM1	6 Mar 2020 15:18:46.684 UTCG	2458915.13804032	0.1042
TCM2	25 Sep 2020 11:59:59.979 UTCG	2459117.99999976	0.1309
TCM3	22 Jul 2021 12:00:00.012 UTCG	2459418.00000013	0.3551
TCM4	22 Jul 2023 12:00:00.000 UTCG	2460148	1.0372

The TCMs start small, but TCM4 ends up being quite large. This is due in part to the ephemerides being

used in the Lambert solution (Meeus) versus in STK (DE421). The initial TCMs have smaller adjustments to make due to the time and distance scales being small. TCM4 corrects a segment that goes much farther and takes more time, enhancing the error between the ephemerides. The Lambert solution assumed simple two-body motion, whereas STK's heliocentric propagator includes the gravity effects from all the planets. The TCMs could be smaller if the Lambert solver and STK ephemerides were the same. In addition, a smaller-granularity Lambert solution window for all planetary encounters could allow for better planetary targeting.

The trajectory has been visualized in Figures 5 and 6 below.

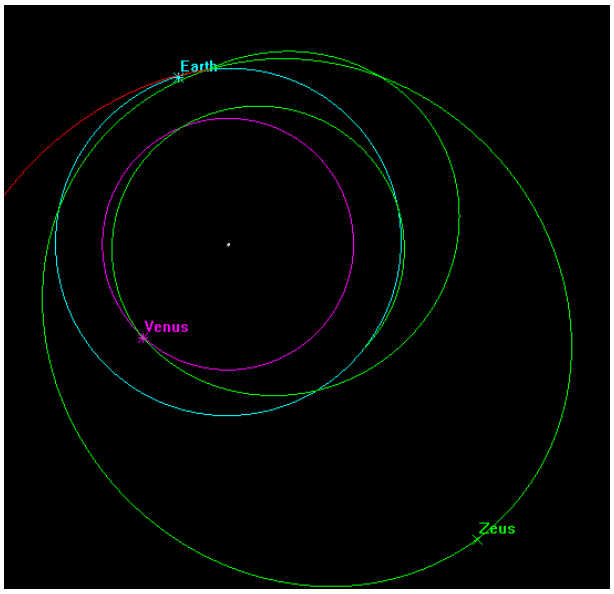

(a) Above Ecliptic

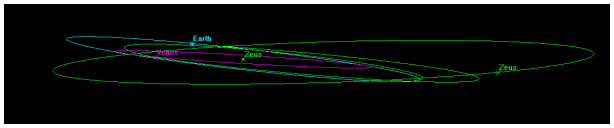

(b) Side view

Figure 5. Inner Trajectory.

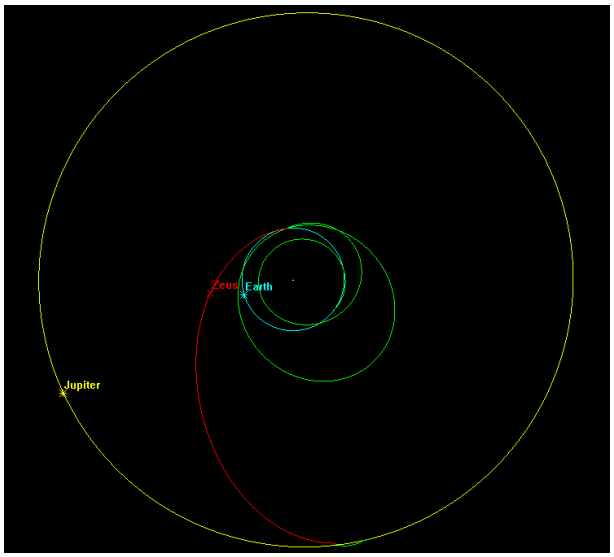

(a) Above Ecliptic

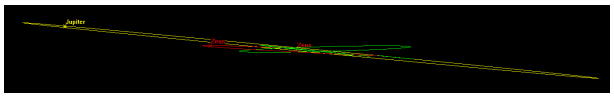

(b) Side view

Figure 6. Outer Trajectory.

The STK-visualized trajectory looks as expected. There is a Type II trajectory from Earth to Venus, Type II from Venus to Earth, a resonant orbit that goes beyond Earth's, and a Type I trajectory to Jupiter. The trajectory from Earth to Jupiter almost looks like a Hohmann transfer, but with a significantly less launch C_3. The JOI and initial Jupiter orbit can be seen in Figure 7 below.

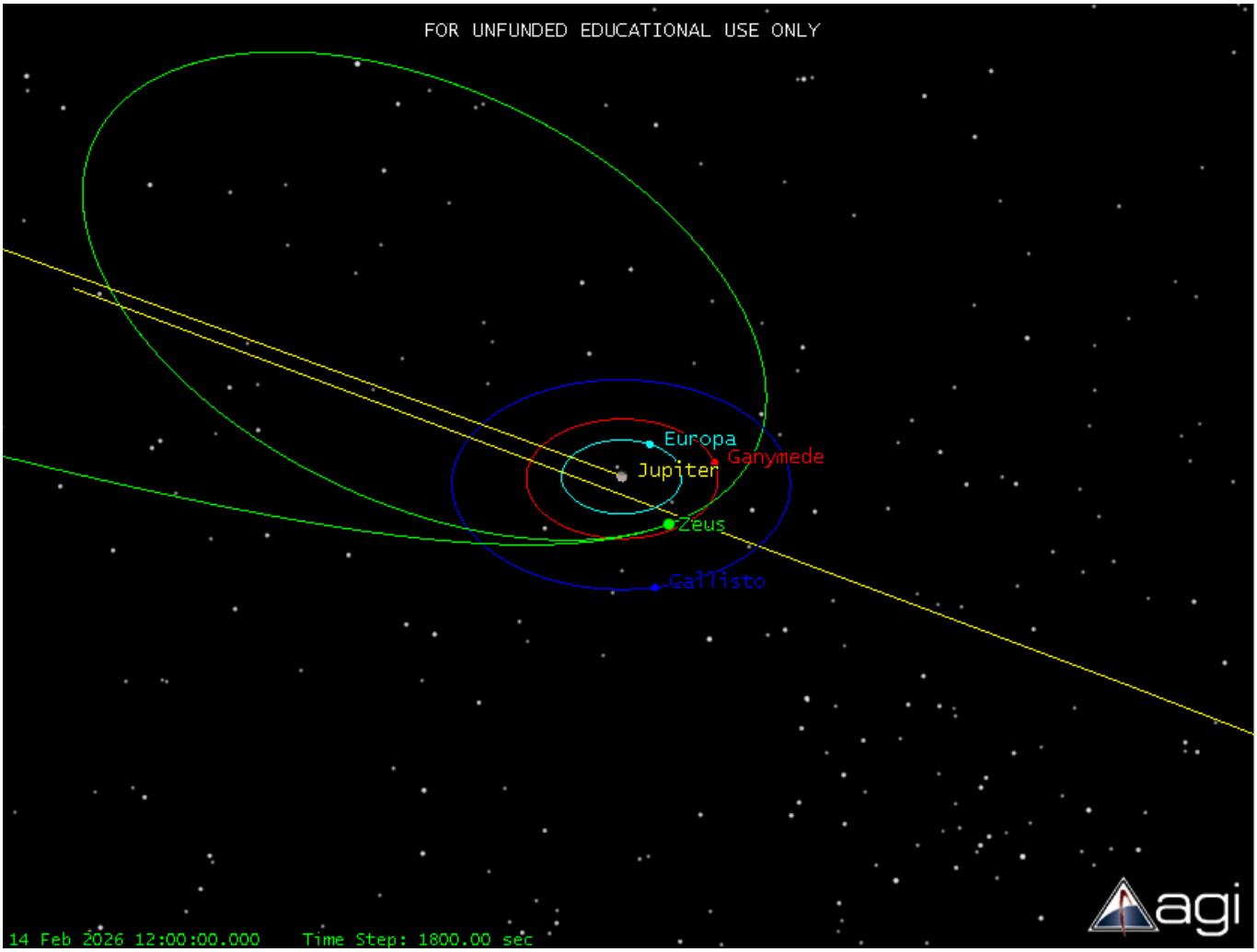

Figure 7. JOI and initial orbit.

The B-plane target was chosen to be the $\left|\vec{B}\right|$ found in the trajectory design, applied entirely in $+\hat{T}$. A positive value of $\hat{T}$ was necessary for prograde motion around Jupiter, since its tilt with respect to the ecliptic plane is small. This resulted in a small inclination (2°) and a period of 142.33 days. The orbit intersects with Ganymede, which will allow for apojove-lowering maneuvers.

IV. Earth Access

Earthly access to a spacecraft is an important aspect of the mission. Software can be uploaded, commands sent, telemetry recieved, and emergencies abated as long as a ground station and the spacecraft have an onobstructed view of one another. It is desirable to see the spacecraft during maneuvers for navigation purposes so that the resulting state can be reconstructed. Figure 8 shows the ground track during the first week of the mission, along with the Deep Space Network (DSN) ground stations.

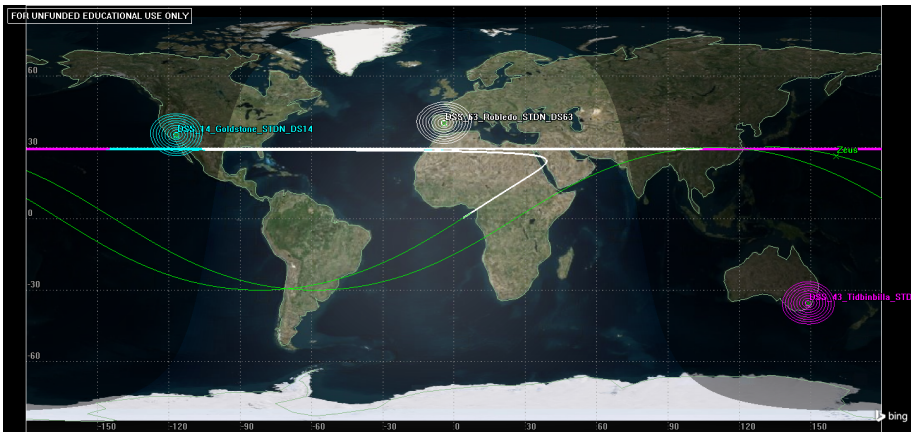

Figure 8. Week 1 ground track.

The spacecraft is visible from the Madrid facility during launch injection, ascertained by the white access line on the ground track. As the craft leaves the earth, it has retrograde motion on the ground track. The first week of DSN access can be seen in Figure 9.

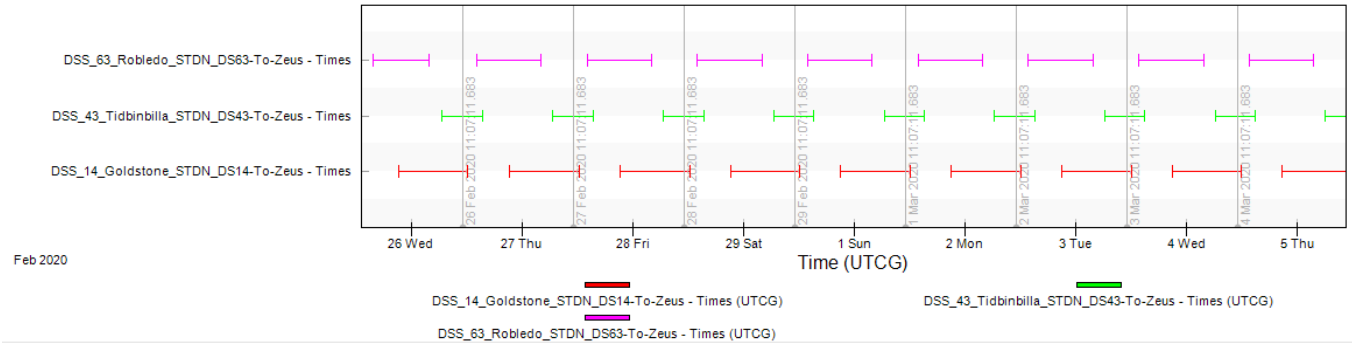

Figure 9. Week 1 DSN access.

The spacecraft is visible to the DSN with at least one station for the rest of the week. Sometimes there is double-coverage available by the facilities.

The Venus gravity assist DSN access is visualized in Figure 10.

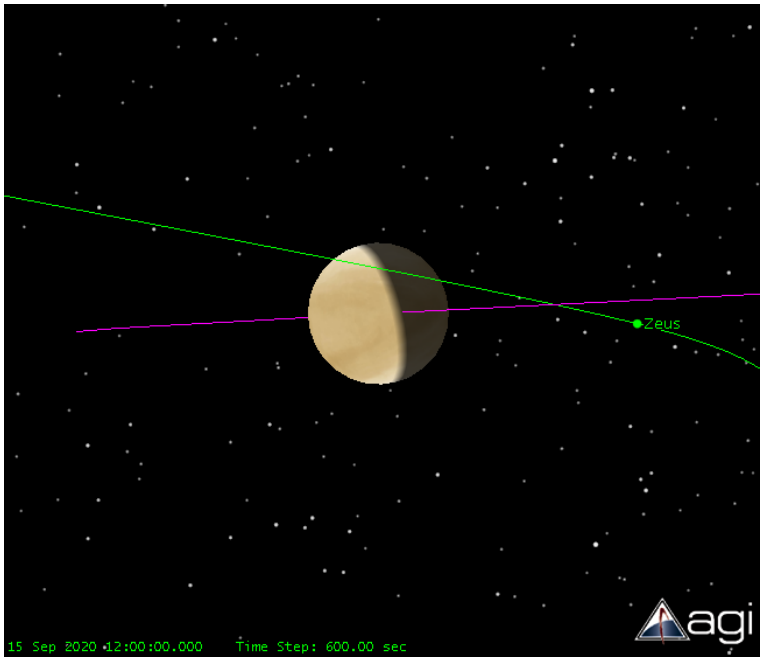

(a) VGA as seen from Earth

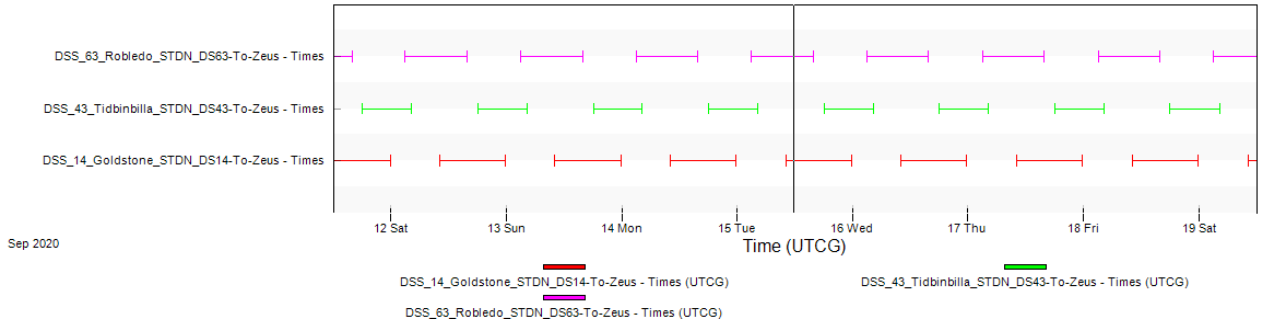

(b) VGA DSN access

Figure 10. VGA visibility to the DSN.

The VGA is most visible from Madrid. One could note that even if Venus obstructed the spacecraft view during closes approach, the spacecraft would be visible quite soon after. In fact, the access scenario is worst-case when the sun is in conjunction with the maneuver. A mission planner should take this into account when designing gravity assists, as there could be adverse impacts on the navigation solution if the maneuver wasn't executed as planned.

The first Earth gravity assist's DSN access is visualized in Figure 11.

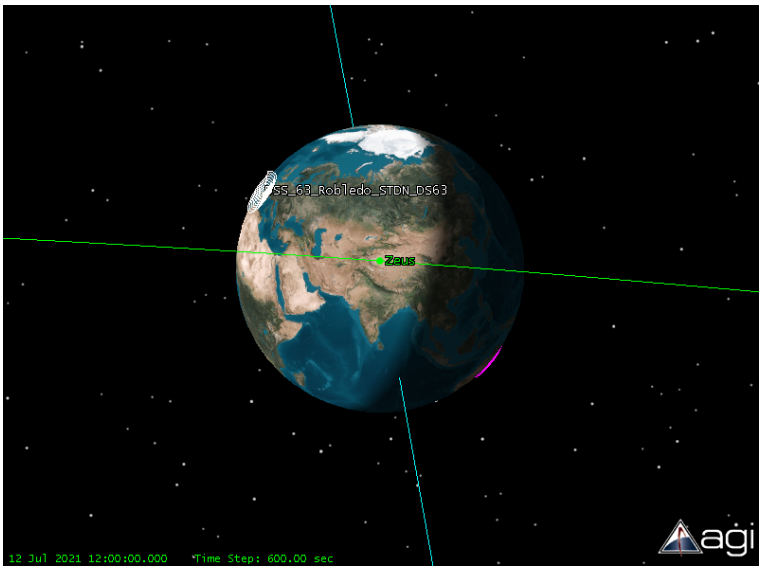

(a) EGA1 closest approach

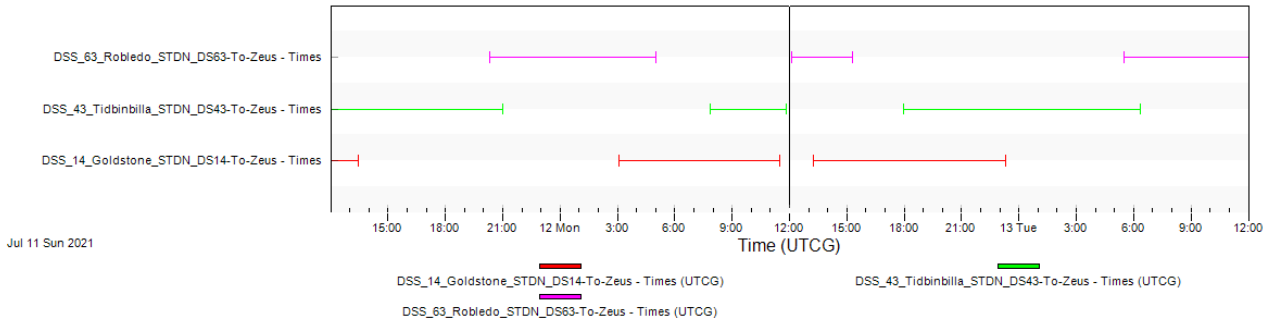

(b) EGA1 DSN access

Figure 11. EGA1 visibility to the DSN.

EGA1 is not visible at the closest approach. However, there are long access periods immediately before and after the maneuver.

The second Earth gravity assist's DSN access is visualized in Figure 12.

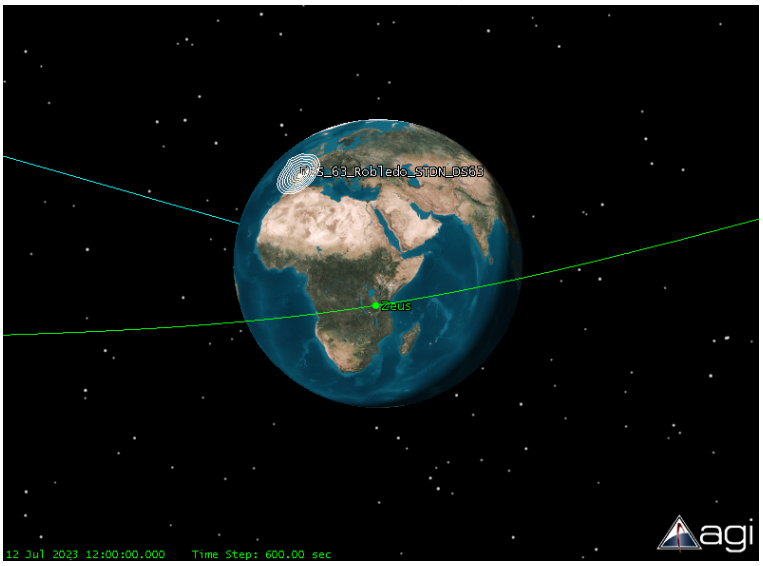

(a) EGA2 closest approach

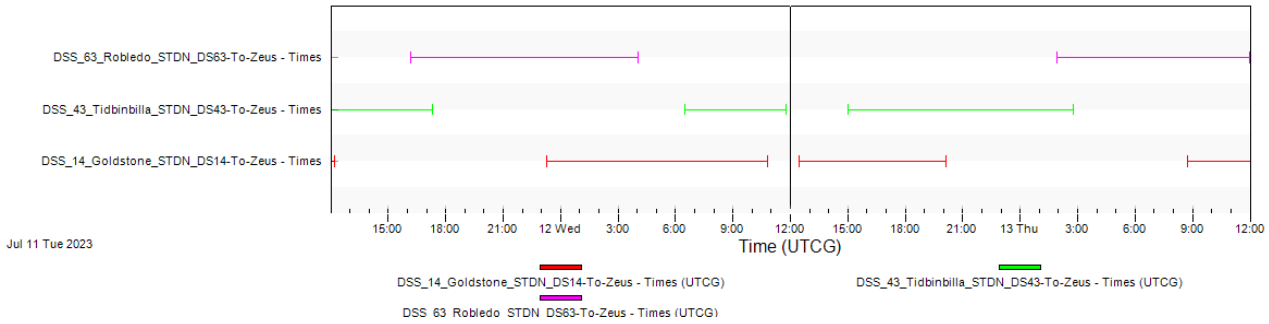

(b) EGA2 DSN access

Figure 12. EGA2 visibility to the DSN.

Again, the Earth gravity assist is not visible to the DSN at the closest approach. From the trajectory figures, one can see that unless the closest path is either above low Earth orbit or it passes directly over a DSN station, it will probably not be visible to the DSN. There are also other factors to consider with DSN access during Earth flybys. The first is that the groundstation antenna in use can move fast enough to maintain contact. In this case, an omnidirectional antenna may be better than the large, high-gain antennas the DSN is famous for. Secondly, the flyby occurs quickly. This means that a body-fixed antenna would need a large attitude maneuver, or a phased array would need to move fast enough to support the access. This is an example of how mission design trickles down into spacecraft subsystem requirements.

Jupiter orbit insertion access is shown in Figure 13.

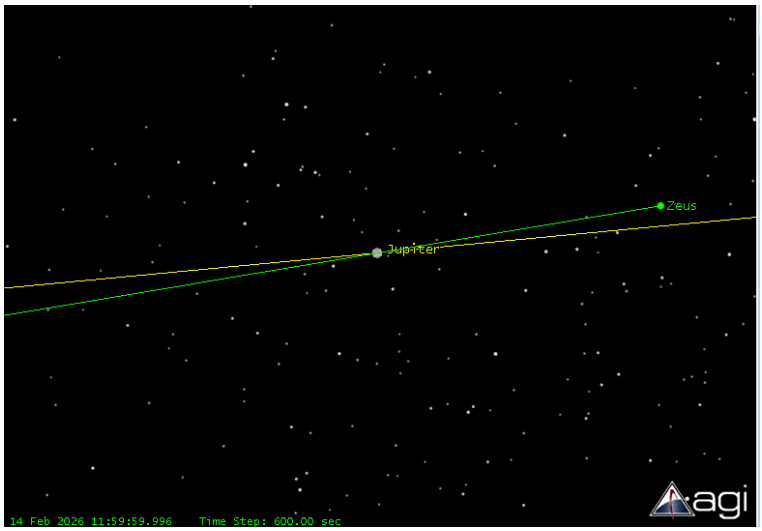

(a) EGA2 closest approach

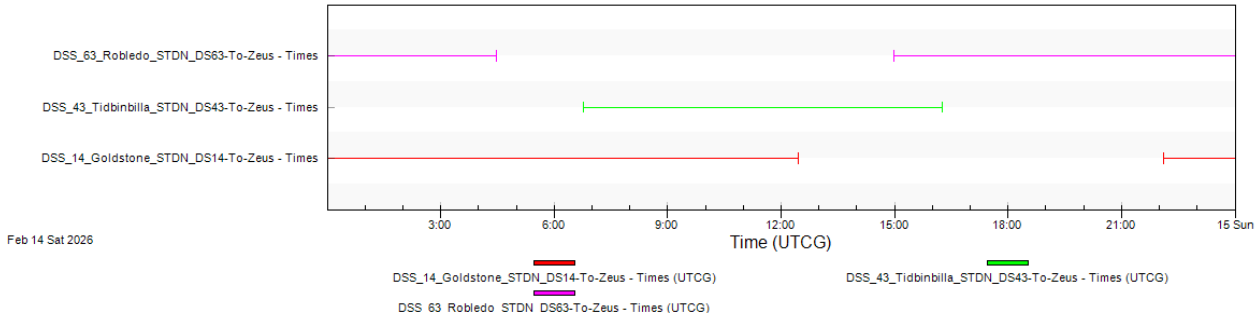

(b) EGA2 DSN access

Figure 13. JOI visibility to the DSN.

The DSN covers the JOI easily, since the DSN geometry can see spacecraft at all longitudes beyond geostationary orbit. The ground track up to and including the JOI is shown in Figure 14.

Figure 14. JOI Ground Track.

DSN access can be seen with the lines connecting the ground station to the spacecraft. If one desired Goldstone-Madrid coverage instead of Goldstone-Canberra coverage, they could move the targeted JOI encounter. For this study, the JOI was moved to 14 Feb 2026 03:00:00 UTCG. The resulting ground track is shown in Figure 15.

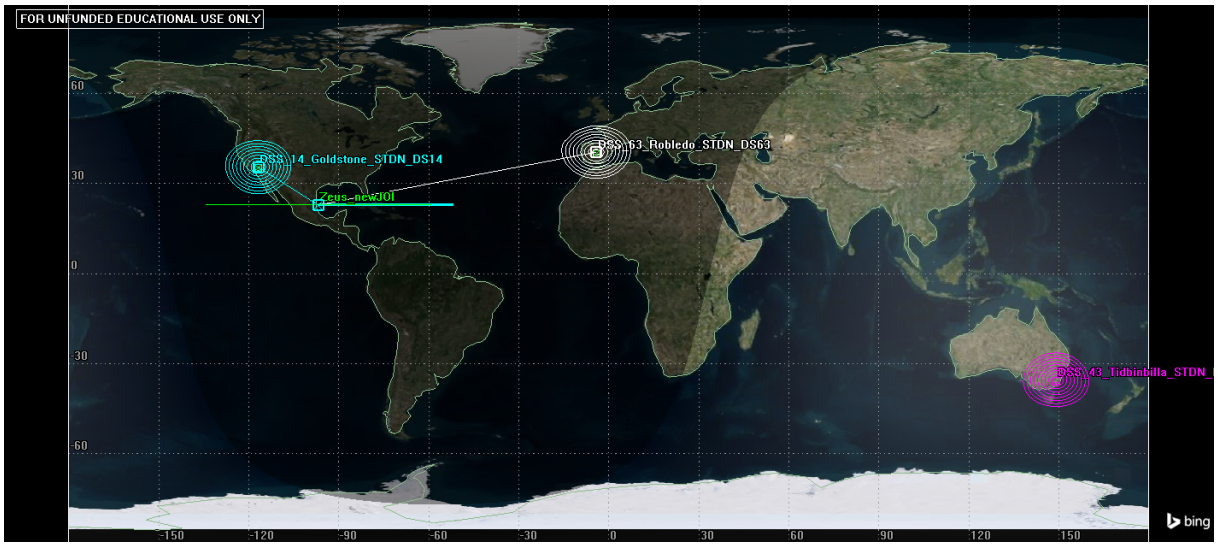

Figure 15. JOI Ground Track, Goldstone-Madrid coverage.

DSN access to the JOI is easy to maintain due to the geometry of the transfer. The spacecraft has a smaller heliocentric velocity than Jupiter at the end of the transfer, requiring the spacecraft to lead the planet. The large $+\hat{T}$ target on the B-plane, which is required for prograde motion about Jupiter, points toward the inner solar system. This means that Jupiter will be in opposition, rather than in conjunction, of the spacecraft, making it visible to the DSN all the way up to JOI. B-plane targets closer to Jupiter could shift JOI out of view, however. This is due to the greater turning angle of the spacecraft as the perijove decreases.

V. Europa Injection

VI. Conclusion

The non-optimal controller was able to meet the design criteria without observer errors. However, it proved to not be as robust to such errors as the LQR controller. This is due to the control effort used in both controllers. The LQR design assigned a cost to control effort, so less was used. On the other hand, the non-optimal controller, which was tuned with SISO methods, was otherwise sufficient in meeting control objectives. Perhaps with sensor filtering, observer error could be reduced such that the control effort would also be reduced.

The Luenberger observer was able to reconstruct the entire state from only knowing the sun angle. The poles also drove initial (realistic) initial observer error to zero without forcing the actuator to violate its constraints.

The state feedback mitigated control of the disturbance. Without the integral term, the steady-state error would be untenable for a sailcraft to get the expected thrust. The feedback on the rest of the state ensured a quick rise that did not exceed the defined overshoot limit.

The control methods presented were able to meet the design criteria for single-axis control of the specified solar-sail spacecraft. Further research should be done for both 2-axis gimballing and combining a gimbal with sail vanes at the edges of the sail, as well as craft with more massive busses and perhaps a gimballed

payload on the other side of the sail. With such research, design flexibility will allow viable missions with reduced time or resource cost.

References

[1]Wie, B., "Solar Sail Attitude Control and Dynamics, Part 2," *Journal of Guidance, Control, and Dynamics*, Vol. 27, 2004, pp. 536–544.

[2]D'Amario, L. A., "Galileo Trajectory Design," *Space Science Reviews*.

[3]Vallado, D. A., *Fundamentals of Astrodynamics and Applications*, Microcosm Press, Hawthorne, CA, 2013.